Estimating the Uncertainty in Passive-Microwave Rain Retrievals

DOROTHÉE COPPENS, ZIAD S. HADDAD, AND EASTWOOD IM

Jet Propulsion Laboratory, California Institute of Technology, Pasadena, California

(Manuscript received 7 June 1999, in final form 28 January 2000)

ABSTRACT

Current passive-microwave rain-retrieval methods are largely based on databases built offline using cloud models. Since the vertical distribution of hydrometeors within the cloud has a large impact on upwelling brightness temperatures, a forward radiative transfer model can associate microwave radiances with different rain scenarios. Once such a database is available, to estimate the rain from measured brightness temperatures, one would look for the rain scenarios in the database whose associated radiances are closest to the measurements. To understand the uncertainties in this process, the authors have restricted their attention to tropical ocean cases and analyzed the marginal and joint distributions of the radiances observed by the Tropical Rainfall Measuring Mission (TRMM) satellite's passive-microwave imager and of those in the databases used in the TRMM passive rain retrieval. The authors also calculated the covariances of the rain profiles and brightness temperatures in the TRMM passive-microwave database and derived a simple parametric model for the conditional variance, given measured radiances. These results are used to characterize the uncertainty inherent in the passive-microwave retrieval.

1. Introduction

Most instantaneous passive-microwave rain-retrieval algorithms currently implemented use a cloud database constructed offline (Kummerow et al. 1996; Kummerow and Giglio 1994a,b; Smith et al. 1994; Tesmer and Wilheit 1998). The databases associate calculated microwave brightness temperatures to sample rain events representing those that are expected to produce the eventual measurements, namely, in our case, precipitation over the tropical ocean. Once a representative database is constructed, one processes each set of instantaneous measurements by searching the database for those scenarios whose associated radiances are closest to the measurements. The details of the search and eventual estimation procedures differ from one retrieval algorithm to the other, but the general principle is the same. In the case of the Tropical Rainfall Measuring Mission's (TRMM) Microwave Imager (TMI), the passive-microwave instantaneous retrieval algorithm uses a large database (Kummerow et al. 1996), which was constructed using various cloud model simulations (Soong and Tao 1984; Tripoli 1992). Radiative transfer calculations followed by the appropriate filters were used to associate to each simulated rain event (itself consisting of surface wind and temperature and relative humidity and hydrometeor profiles, all area-averaged to match the TMI resolution) the brightness temperatures that one would expect the TMI's 10.7 GHz H- and V-pol, 19.3 GHz H- and V-pol, 21.3 GHz V-pol, 37 GHz H- and V-pol, and 85.5 GHz H- and V-pol channels to measure.

Given a set of measured radiances, one hardly ever expects to find in one's database exactly matching calculated brightness temperatures. It is therefore important to be able to estimate the ''spread'' of the closest near-matches that one does find. To quantify this uncertainty, we start by studying the joint behavior of the brightness temperatures and of the rain in the vertically layered atmosphere. The results are used to quantify the conditional variance of the estimated rain given a set of microwave radiances. They are also used to compute the conditional covariance of the brightness temperatures given the rain, as knowledge of this covariance is crucial to those retrieval algorithms such as the currently implemented TMI's (Kummerow et al. 1996), which rely on Bayes' reformulation of the desired probability $p(\mathbf{R} \mid \mathbf{T}_b)$ for the rain $\mathbf{R}$ given brightness temperatures $\mathbf{T}_b$ in terms of the more readily computable probability $p(\mathbf{T}_b \mid \mathbf{R})$ for the brightness temperatures given the rain:

$$p(\mathbf{R} \mid \mathbf{T}_b) = p(\mathbf{T}_b \mid \mathbf{R}) p_{\text{prior}}(\mathbf{R}) \qquad (1)$$

[here, ''$p_{\text{prior}}(\mathbf{R})$'' represents any a priori knowledge about the rain; in practice, p_{prior} would be an archival lognormal distribution if no independent information about $\mathbf{R}$ is available].

The main obstacle to conducting these studies is the

Corresponding author address: Dr. Ziad S. Haddad, Jet Propulsion Laboratory, MS 300-227, 4800 Oak Grove Drive, Pasadena, CA 91109-8099.
E-mail: Ziad.S.Haddad@jpl.nasa.gov

large number of variables for which one has to account. In section 2, we begin by studying the vertically stratified rain by itself in order to derive an economical representation of the rain profiles. In section 3, we study the brightness temperatures and derive expressions for the conditional covariances on both sides of (1). In section 4, we further use our results to derive first-order parametrized retrieval formulas that estimate rain rates and their uncertainties from measured brightness temperatures.

2. Principal component analysis of the vertical rainfall *R*

The passive-microwave TRMM cloud-simulations database represents rain profiles by stratifying the atmosphere into 14 homogeneous layers, of which 8 are below the typical 4.5 km freezing level in the Tropics. This implies that one would require at least eight variables to describe the liquid rain for each profile. A principal value analysis reveals that this number can be reduced. Indeed, calling $R_1, \ldots, R_8$ the rain in the first eight 0.5-km layers above the surface (numbered from the surface up), one can compute the covariance matrix of these variables from one's database and diagonalize it. The matrix of change of basis specifies which eight (new) linear combinations of the R_i's are mutually uncorrelated, and the associated eigenvalues determine the amount of information carried by each of the new variables. Large eigenvalues indicate a correspondingly large variation in the associated variable while smaller eigenvalues indicate that the value of the corresponding variable changes relatively little over the whole data. In practice, we calculated the covariance matrix of $\log(R_i)$ for the TRMM cloud-simulations database and then diagonalized it. The main result is that the largest eigenvalue is significantly larger than the remaining seven, and its eigenvector is very close to $R_1' \cong (1/\sqrt{8}) \sum_1^8 \log R_i$. The eigenvalues were

$$45 > 0.51 > 0.054 > 0.0024 > \cdots > 3.4 \times 10^{-6},$$

suggesting that the last seven eigenvariables [here r stands for $\log(R)$];

$$R_2' = 0.38r_1 + 0.35r_2 + 0.26r_3 + 0.15r_4 + 0.006r_5 - 0.18r_6 - 0.41r_7 - 0.67r_8, \quad (2)$$

$$R_3' = -0.5r_1 - 0.29r_2 + 0.03r_3 + 0.31r_4 + 0.454r_5 + 0.37r_6 + 0.04r_7 - 0.47r_8, \quad (3)$$

$$R_4' = 0.47r_1 - 0.08r_2 - 0.46r_3 - 0.38r_4 + 0.043r_5 + 0.42r_6 + 0.34r_7 - 0.35r_8, \quad (4)$$

$$R_5' = -0.4r_1 + 0.50r_2 + 0.28r_3 - 0.28r_4 - 0.374r_5 + 0.11r_6 + 0.44r_7 - 0.24r_8, \quad (5)$$

$$R_6' = 0.21r_1 - 0.46r_2 + 0.19r_3 + 0.40r_4 - 0.35r_5 - 0.31r_6 + 0.53r_7 - 0.20r_8, \quad (6)$$

TABLE 1. The rms error on the rain rate estimated for each layer from the mean rain rate R_1' and $\mathcal{E}\{R_2'\}, \ldots, \mathcal{E}\{R_8'\}$.

	rms deviation (mm h^{-1})	Mean relative deviation (%)
R_1	1.2675	12.99
R_2	1.1499	11.27
R_3	0.8296	8.35
R_4	0.5173	6.03
R_5	0.4205	5.39
R_6	0.6077	7.31
R_7	0.9812	13.07
R_8	1.3320	23.63

$$R_7' = -0.1r_1 + 0.38r_2 - 0.52r_3 + 0.19r_4 + 0.367r_5 - 0.55r_6 + 0.31r_7 - 0.07r_8, \quad (7)$$

$$R_8' = 0.06r_1 - 0.23r_2 + 0.45r_3 - 0.57r_4 + 0.513r_5 - 0.35r_6 + 0.16r_7 - 0.04r_8, \quad (8)$$

could be considered constant without incurring a very large error in the description of the rain. The vertical distribution of rain in the atmosphere could thus be described to first order by the vertically averaged rain rate R_1' and the constant values of the means of $R_2', \ldots, R_8'$.

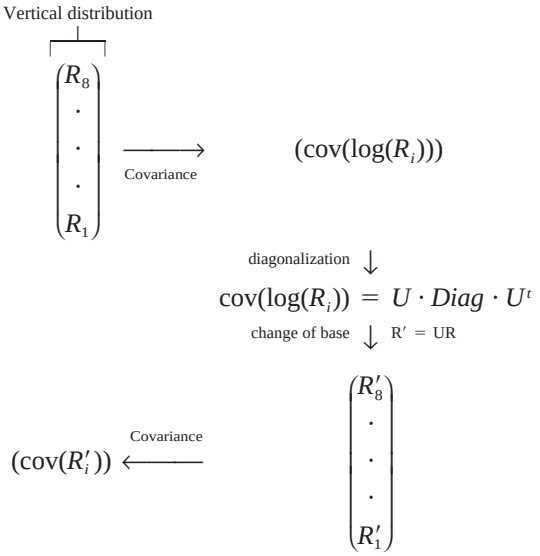

Indeed, when reconstructed using R_1' and the mean values $\mathcal{E}\{R_2'\} = 0.0635$, $\mathcal{E}\{R_3'\} = 0.0432$, $\mathcal{E}\{R_4'\} = -0.003$, $\mathcal{E}\{R_5'\} = -0.0002$, $\mathcal{E}\{R_6'\} = -0.0001$, $\mathcal{E}\{R_7'\} = -0.00004$, and $\mathcal{E}\{R_8'\} = -0.00007$, the values for the rain rates were within 24% of the original values. Table 1 shows the individual results for each of the eight layers, and Fig. 1 illustrates the case of the near-surface layer.

In order to verify that this high correlation between the rain in the various layers is not due to an artifact of the cloud models used to generate the TRMM passive-microwave database in the first place, a similar analysis

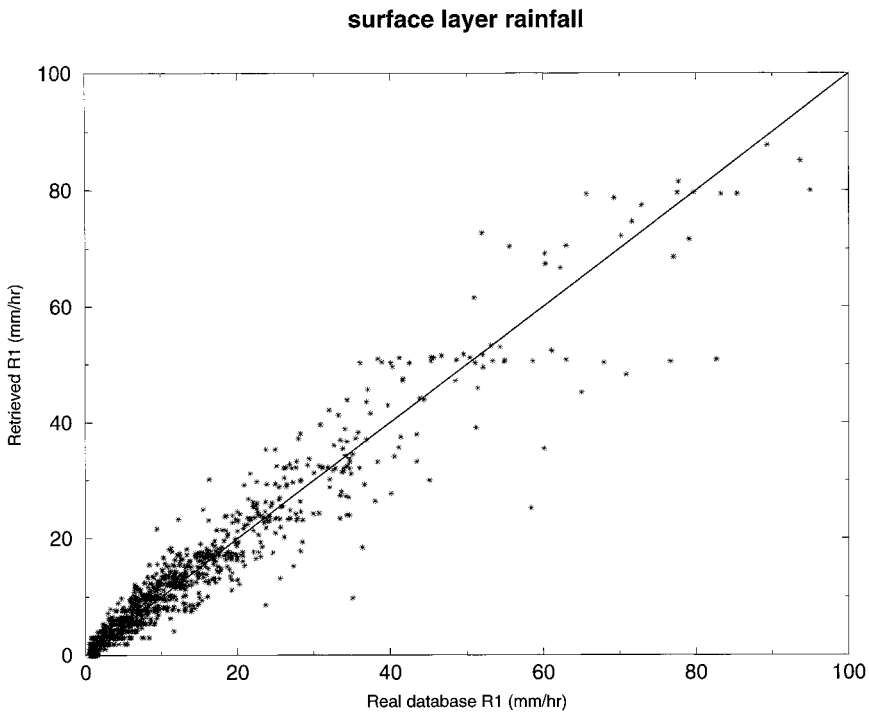

FIG. 1. Near-surface R_1 retrieved from R_1'.

was applied to actual data from the TRMM radar. We analyzed the data from 60 orbits completed in Sept 1998. The natural logarithms of the rain-rate estimates of the TRMM-combined algorithm (Haddad et al. 1997) for the fourteen 250-m layers between 750 m and 4 km were used. The first three altitude bins near the surface were ignored to avoid surface clutter problems. The covariance matrix was calculated and diagonalized. The results obtained are quite similar to the ones found for the passive microwave database rain rates. For convective events, the eigenvalues were $12.46 > 5.1 > 0.94 > 0.3 > \cdots > 1 \times 10^{-2}$. The coefficients of the eigenvector $\Sigma_i a_i \log(R_i)$ for the first eigenvalue 12.46 all verified $0.17 < a_i < 0.3$, quite close to the value $1/\sqrt{14} \simeq 0.267$. Hence, R_1' is indeed very close to the vertically averaged rainfall. The eigenvalues in the stratiform case were similar to those in the convective case: $7.6 > 1.86 > 0.4 > 0.14 > \cdots > 8 \times 10^{-3}$. The coefficients of the eigenvector $\Sigma_i a_i \log(R_i)$ corresponding to the first eigenvalue were in the range $0.21 < a_i < 0.29$. Merging all cases together, the eigenvalues were $11.8 > 0.43 > 0.14 > \cdots > 9 \times 10^{-3}$, with an eigenvector $\Sigma_i a_i \log(R_i)$ for the first eigenvalue satisfying $0.21 < a_i < 0.29$. As in the case of the passive-microwave database, the first eigenvalue is far bigger than the remaining ones, although since we do have 14 layers, the second eigenvalue could not be negligible. It is particularly interesting to note that for the convective, stratiform, or all merged events, the eigenvector $\Sigma_i b_i \log(R_i)$ for this second eigenvalue always had the form $(b_1, \ldots, b_7, -b_8, -b_9, \ldots, -b_{14})$, with $0.13 < b_1, \ldots, b_6, b_9, \ldots, b_{14} < 0.34$ and $b_7 \cong b_8 \cong 0.05$. In other words, the second eigenvector quantifies the difference between the rain below 2.25 km and the rain above 2.75 km. This is remarkably similar to the case of the TRMM cloud-simulations database; indeed, (2) specifies that the second eigenvector for the rain described in the database is the difference between the rain below 2 km and the rain above 2.5 km. Figure 2 shows the scatter diagram of the first two eigenvectors in the cases of the TRMM passive-microwave database and of some TRMM radar data obtained during 10 orbits in Jan 1999. In both cases, the second eigenvector varies most (and is therefore most descriptive) for the moderate rain rates. This is consistent with the fact that near-surface evaporation can be significant, especially under stratiform rain, a process that is best quantified by the difference between the rain aloft and the rain near the surface. In summary, our principal component analysis confirms that the TRMM passive-microwave database is consistent with measurements in the Tropics and suggests that in the Tropics, one should be able to describe the vertical distribution of rain using two variables only: the mean rain rate (the first eigenvector) and the difference between the rain in upper and lower layers.

3. Conditional covariances of R and T_b

Since it is almost always impossible to find an exact match for a set of measured radiances in one's database,

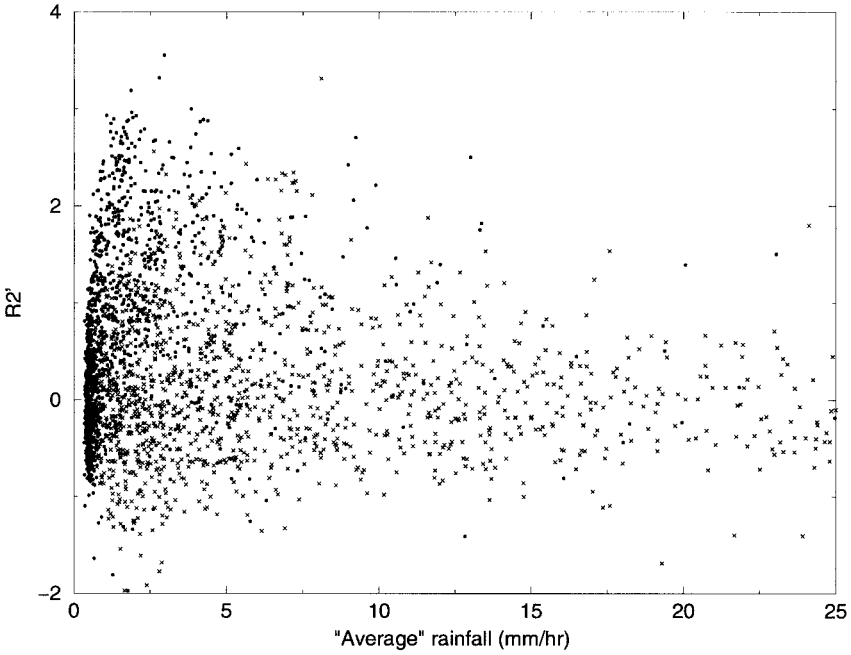

FIG. 2. The term R_2' vs $\exp(R_1'/\sqrt{N})$, with $N = 8$ for the database ($\times$) and $N = 14$ for the TRMM radar ($\bullet$).

one must quantify the conditional covariances of the variables in the database in order to estimate the uncertainty in any rain retrieval based on the database. In the previous section, in the course of the principal component analysis, we verified that the joint behavior of the TRMM database rain rates at different heights is almost identical to that of the (independent) estimates of the TRMM radar. Before proceeding to the calculation of the conditional covariances, we must check that the TRMM database brightness temperatures are also consistent with the TRMM observations, which we did by analyzing the TMI data obtained during 6 orbits on 7 and 18 Oct 1998. For each of the 85.5-GHz channels, we had 113 007 rain and 2 521 922 clear-air samples while for each of the other (lower resolution) channels, we had 64 338 rain and 1 253 154 clear-air samples. Figure 3 shows the 10.7 GHz V-pol histograms of the measurements and of the database samples, for no-rain events as well as for rain cells. Since the database does not contain any clear-air samples per se, that histogram was constructed using those samples for which the rain rate did not exceed 0.25 mm h^{-1} anywhere in the rainy

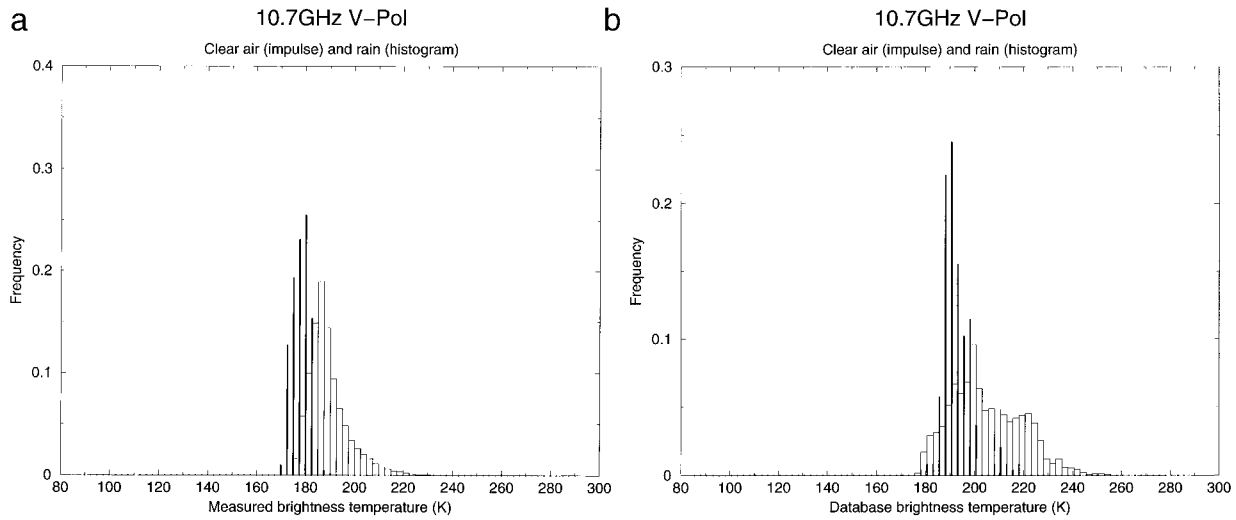

FIG. 3. Comparison of the 10.7-GHz T_b histograms.

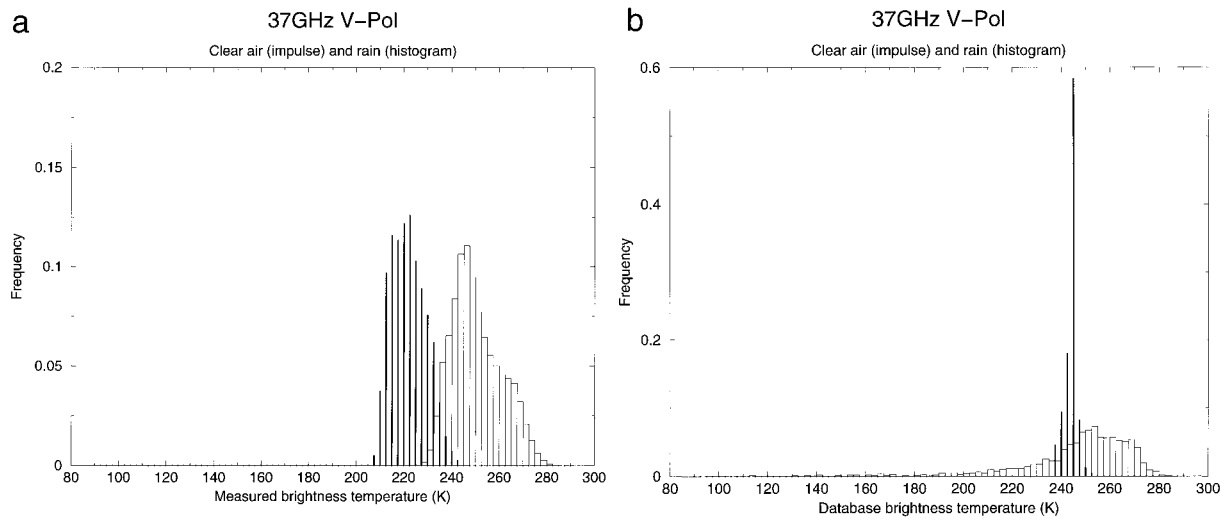

FIG. 4. Comparison of the 37-GHz T_b histograms.

column. This explains the small positive bias of the clear-air database histogram compared with the measurements. The rainy samples, however, show remarkable large-scale agreement with the data, although there is a notably larger incidence of high brightness temperatures in the database. This is most likely due to the database's emphasis on substantial convective precipitation and a corresponding probable underrepresentation of stratiform rain. The same features are evident in the histograms for the 10.7-H, 19.3-H, 19.3-V and 21.3-V channels. At 37 GHz (Fig. 4), the database contains a relatively small but significant number of rain samples with low associated brightness temperatures extending well below the clear-air values, while no measurements fell in this region. This feature is more pronounced in the 85.5 GHz (Fig. 5), where the database contains no rain samples with brightnesses exceeding the clear-air cases, while the measurements actually peak in that region. This is an indication that the database overrepresents high-scattering events, as noted earlier, and that scattering is overestimated in the radiative transfer calculations (because of an overproduction of ice, nonrepresentative frozen hydrometeor size distributions, or unrealistically slow fall velocities; see, e.g., Panegrossi et al. 1998 for a discussion of some of these effects). A test for goodness of fit for the 37-V data reveals that the (approximately χ^2) statistic

$$\sum_{i=1}^{14} \frac{([\text{No. database samples}]_i - [\text{No. measurements}]_i)^2}{[\text{No. measurements}]_i}, \quad (9)$$

computed using a binning into 2.5-K intervals between 240 and 270 K, has a value of 36.4, which for a χ^2

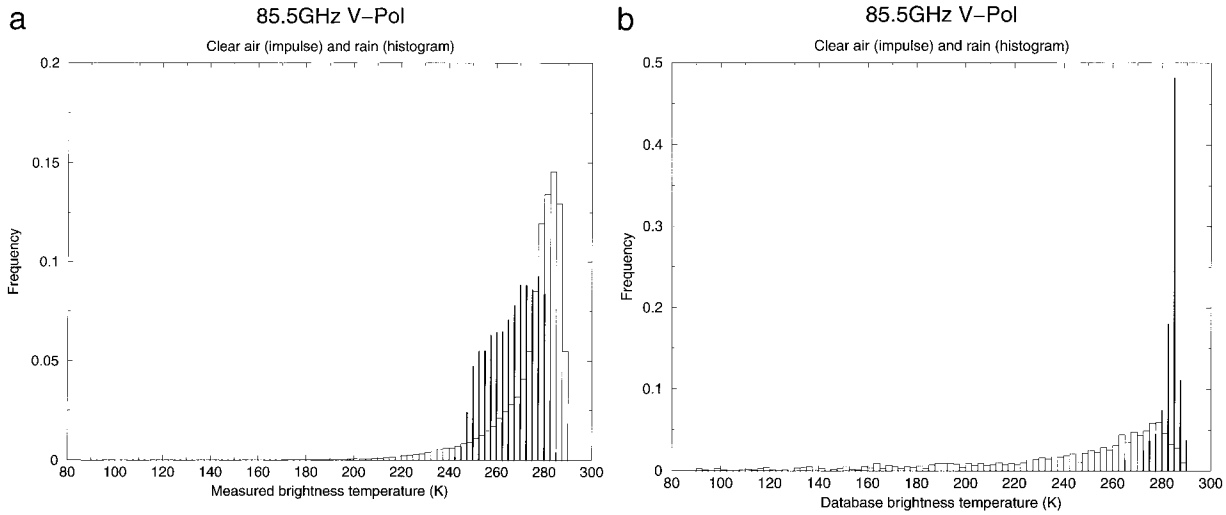

FIG. 5. Comparison of the 85.5-GHz T_b histograms.

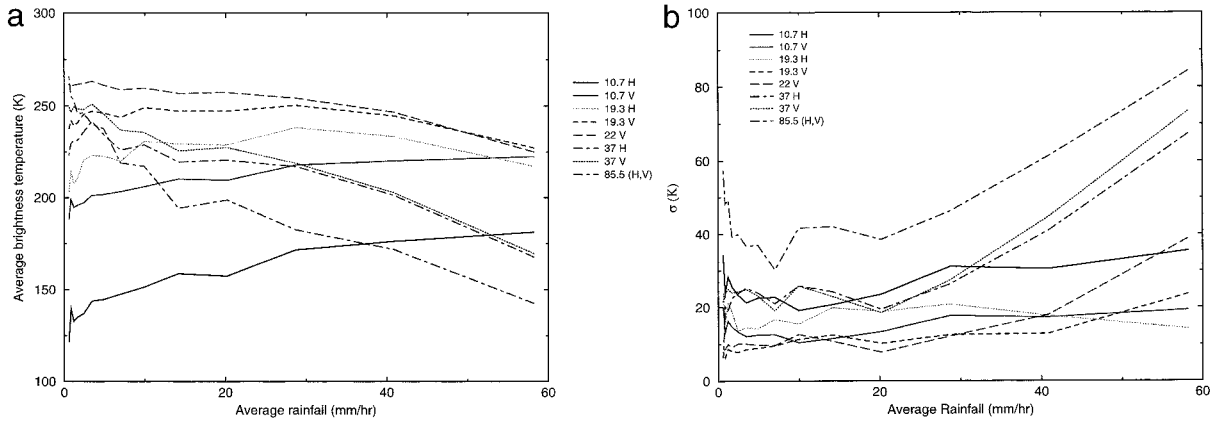

FIG. 6. Means and standard deviations of T_b given an "average" $R = \exp(R_1'/\sqrt{8})$.

variable with 13 degrees of freedom, is at the 99.91st percentile. This value is not as small as one may have liked; while it may have been affected by the very large sample size, which greatly increases the penalty for a mismatch between observations and simulated temperatures, the mismatch seems mostly due to the questionable representativity of the observations themselves. Thus on the whole, while the database temperatures are not totally inconsistent with the observations, the evident mismatches indicate that the current database overemphasizes scattering and/or over-represents high-scattering cases and that it would be prudent to make the database more representative in order to improve our interpretation of the TMI's observations. The "too-much-scattering" problem could be addressed by tuning the frozen hydrometeor size distributions and fall speeds in the cloud models themselves, and the general representativity of the database can be improved by resampling it. These possible remedies, however, require much effort and are quite beyond the scope of the current study.

Figure 6 shows the conditional means $\mathcal{E}\{T_b \mid R_1'\}$ of the brightness temperatures given the "mean" R_1'. Except for the 10.7- and 85-GHz channels, the curves are neither monotone nor do they have a pronounced slope. Figure 6 also shows the conditional root-mean-square (rms) deviations. For light rain, the 85.5-GHz uncertainties are the highest, approaching 60 K, followed by the 10.7 GHz H-pol uncertainty of about 30 K. As the rain increases, the uncertainties initially drop, then increase again once the rain rate exceeds about 10 mm h^{-1}. For large rain rates, the 85.5-GHz uncertainties climb beyond 80 followed closely by the 37-GHz σ's. This is due to the fact that the effect of scattering from ice increases as the frequency increases, while the amount of ice is not closely related to the amount of rain. The uncertainties in the other channels remain below 40 K. Table 2 and Fig. 7, showing the correlation coefficients of the various channels given R_1', complete the description of the conditional covariance. The high correlations between the two polarizations at each frequency are not surprising, since the forward radiative transfer model used to generate the database did not account for any polarization effects except those from the surface. Somewhat more surprising is the sign of the correlation coefficient between 19.3 GHz H-pol and both 21 GHz V-pol and 37 GHz V-pol; for low rain rates, the correlation is close to -1 but it becomes positive for rain rates above about 2.5 mm h^{-1} and approaches $+1$ for high rain rates. More significant is the consistently positive correlation between 19.3 GHz V-pol and the higher-frequency channels, and its relatively weaker correlation with the low-frequency channels. This suggests that in the TRMM database, both 19.3-GHz channels are affected by scattering in the cloud model used even at very low rain rates, the effect being more significant at V-polarization than at H.

To quantify the effect of the ambiguities in the database on the direct retrieval of the rain rates from measured brightness temperatures, we proceed as before and start by reducing the number of variables required to describe the radiances. The eigenvalues of the covariance matrix of the database brightness temperatures turn out to be

$$5652 > 965 > 314.6 > 72.37 > 31.5 > 4.77 > 3.9 > 0.18 > 0.11, \quad (10)$$

with corresponding eigenvectors

$$T_1' = -0.13T_{10}^H - 0.07T_{10}^V + 0.03T_{19}^H + 0.08T_{19}^V + 0.15T_{21} + 0.3T_{37}^H + 0.37T_{37}^V + 0.6T_{85}^H + 0.6T_{85}^V, \quad (11)$$

$$T_2' = 0.7T_{10}^H + 0.4T_{10}^V + 0.5T_{19}^H + 0.26T_{19}^V + 0.07T_{21} + 0.24T_{37}^H + 0.08T_{37}^V - 0.03T_{85}^H - 0.04T_{85}^V, \quad (12)$$

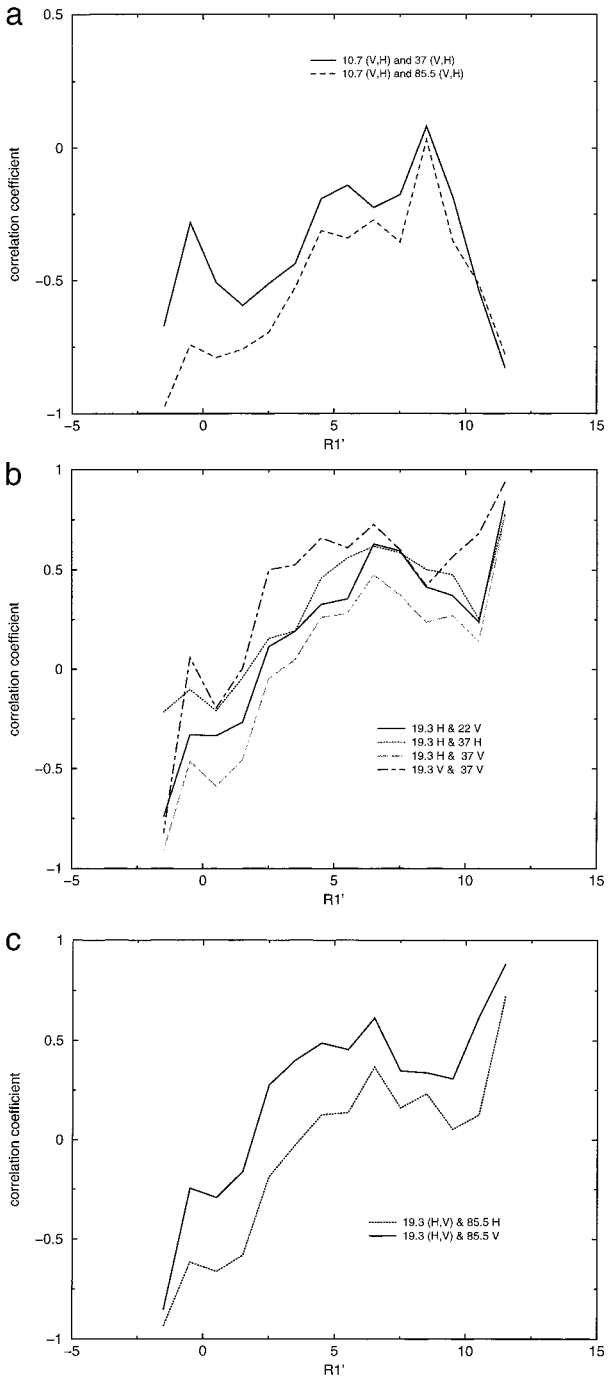

FIG. 7. Correlation coefficients for the passive channels given R_1'.

$$T_3' = -0.42T_{10}^H - 0.2T_{10}^V + 0.2T_{19}^H + 0.265T_{19}^V + 0.34T_{21} + 0.45T_{37}^H + 0.3T_{37}^V - 0.3T_{85}^H - 0.36T_{85}^V, \quad (13)$$

$$T_4' = 0.3T_{10}^H + 0.1T_{10}^V - 0.57T_{19}^H - 0.35T_{19}^V - 0.2T_{21} + 0.45T_{37}^H + 0.4T_{37}^V - 0.135T_{85}^H - 0.17T_{85}^V, \quad (14)$$

$$T_5' = -0.1T_{10}^H - 0.256T_{10}^V + 0.4T_{19}^H - 0.2T_{19}^V - 0.7T_{21} + 0.41T_{37}^H - 0.2T_{37}^V + 0.05T_{85}^H - 0.007T_{85}^V, \quad (15)$$

$$T_6' = 0.47T_{10}^H - 0.8T_{10}^V + 0.1T_{19}^H - 0.2T_{19}^V + 0.25T_{21} - 0.1T_{37}^H + 0.06T_{37}^V - 0.01T_{85}^H + 0.002T_{85}^V, \quad (16)$$

$$T_7' = -0.06T_{10}^H - 0.007T_{10}^V + 0.2T_{19}^H + 0.024T_{19}^V - 0.4T_{21} - 0.5T_{37}^H + 0.7T_{37}^V - 0.1T_{85}^H + 0.02T_{85}^V, \quad (17)$$

$$T_8' = 0.16T_{10}^H - 0.27T_{10}^V - 0.37T_{19}^H + 0.8T_{19}^V - 0.33T_{21} + 0.04T_{37}^H - 0.06T_{37}^V - 0.1T_{85}^H + 0.1T_{85}^V, \quad (18)$$

$$T_9' = 0.02T_{10}^H - 0.05T_{10}^V - 0.04T_{19}^H + 0.14T_{19}^V - 0.07T_{21} - 0.08T_{37}^H + 0.06T_{37}^V + 0.7T_{85}^H - 0.7T_{85}^V. \quad (19)$$

Once again, the eigenvalues decrease quite rapidly, the third one being already more than an order of magnitude smaller than the first. One can therefore quite adequately describe the nine passive-microwave measurements using T_1' (and for additional precision if required, T_2') and the means of the remaining T_i''s. Figure 8 shows the conditional mean of the R_i's given T_1', and Fig. 9 shows the conditional standard deviations. As the figures show, the uncertainties do decrease as the rain itself decreases, but they increase as a proportion of the rain rate. Indeed, the standard deviations are consistently around 55% for the higher rain rates, then rise to about 65% when the rain rates drop to about 20 mm h^{-1} and continue rising as the rain drops, exceeding 100% as soon as the rain rates drop below 20 mm h^{-1} and remaining near 15 mm h^{-1} for the lowest rain rates. Since the rain rate remains positive, much of this deviation must necessarily lie above the mean, making an overestimation of the rain likely if the joint behavior of the database radiances is not consistent with that of the measurements.

4. Estimation of R using microwave brightness temperatures T_b

The principal component analyses allowed us to reduce the number of variables required to describe the rain as well as those required to describe the measured brightness temperatures. It is therefore natural to investigate the possibility of estimating the rain from the measured radiances directly using the reduced set of variables without having to consult a database in real time. Since the vertical distribution of rain can be adequately described using a single variable R_1', the mean rainfall value in the atmosphere, the problem of estimating the rain from a vector of measured brightness temperatures can be reduced to estimating the corresponding value of R_1'. For this application, we chose to consider a higher-resolution

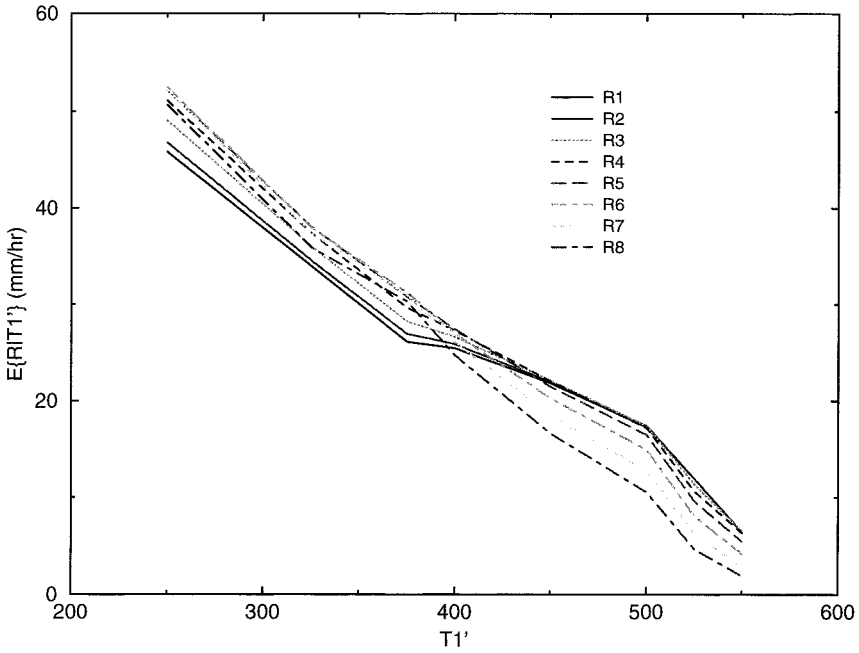

FIG. 8. Means of R given T_1'.

scenario than the previous case of TRMM and used a cloud model simulation of a hurricane implemented on a 3-km grid, with five 1-km rain layers and assuming a nadir look angle. We considered nine channels: 10.7 H, 10.7 V, 19.3 H, 19.3 V, 21.3 V, 37 H, 37 V, 85.5 H, and 85.5 V.

In practice, it would be simplest to use a subset of all available microwave channels to estimate R_1' and thus ''distill'' the information contained in the database into a simple parametrized functional relation. Using an approach similar to the principal component analysis above, we looked for the ''optimal'' linear com-

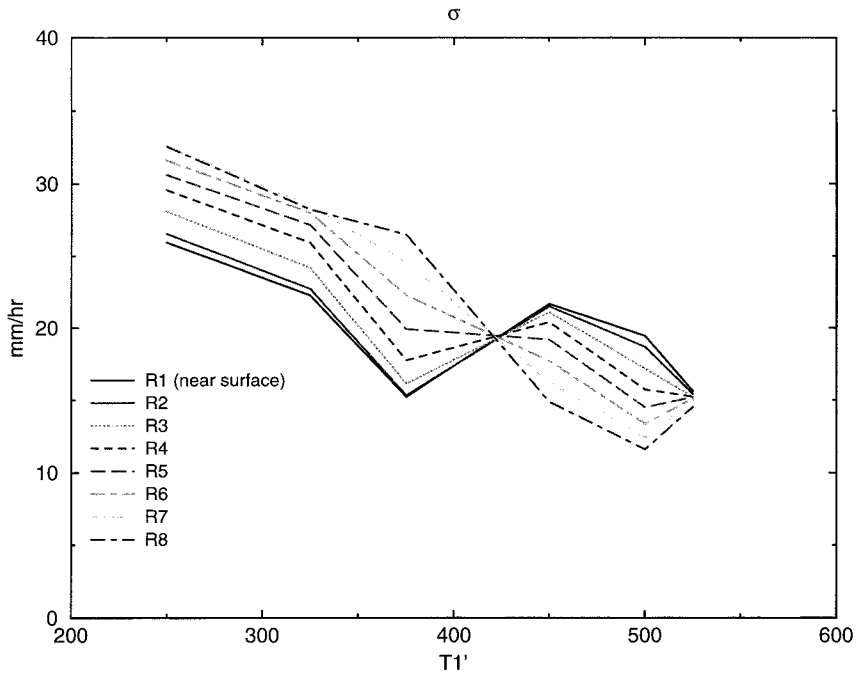

FIG. 9. Root-mean-square variation of R given T_1'.

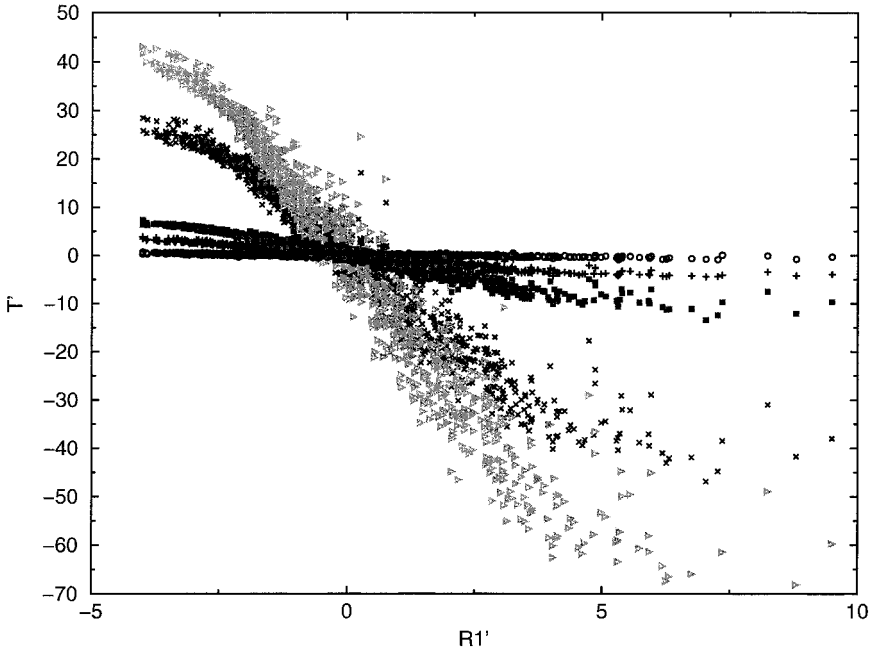

FIG. 10. Selected candidate T''s: T'_{opt} using 4 H-pol with 21.3V (△); all 5 V-pol (×); 4 H-pol with 19.3V (■); 4 H-pol with 10.7V (+); 19.3 V, 19.3 H, 21.3 V, 37 H, and 85.5 H (○).

bination of the passive channels that will ''best'' estimate the rain and quantify the residual ambiguity. Because the problem of finding the best relation between R'_1 and a combination T' of brightness temperatures T_i among 10.7, 19.3, 21.3, 37, and 85.5 GHz is a priori nonlinear, we modify it slightly by trying to maximize the correlation's numerator $E\{R'_1 T'\}$ keeping $E\{T'^2\}$ constant. This, in effect, minimizes the scatter between T' and R'_1. Once the coefficients of T' are found, one can easily compute the mean and variances of R' given T' and thus determine the inverse relation and its uncertainty.

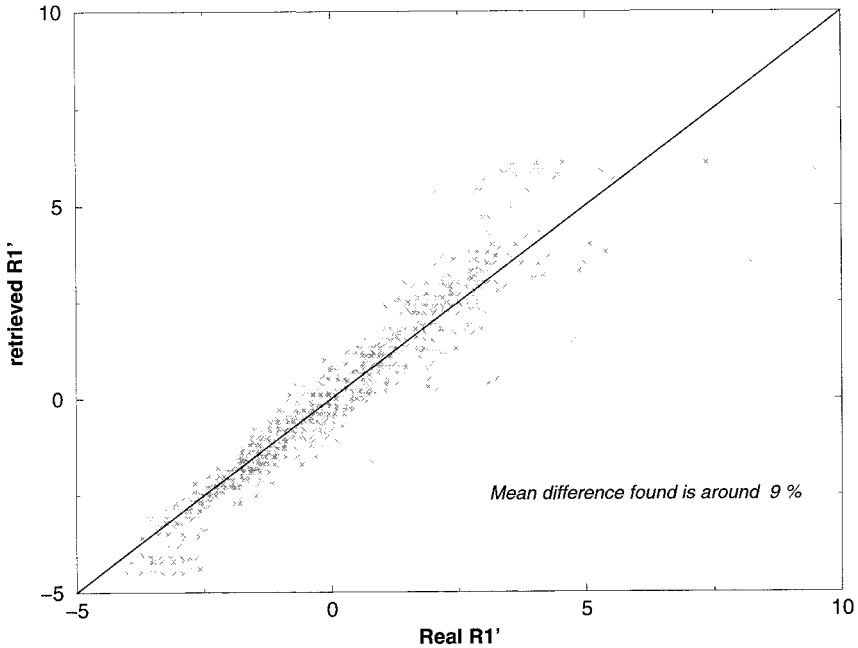

FIG. 11. The quantity R'_1, retrieved from T'_{opt}, vs the actual R'_1.

TABLE 2. Correlation coefficients of T_b given R; most coefficients do not vary significantly with R.

	10.7 V	10.7 H	19.3 V	19.3 H	21.3 V	37 V	37 H	85.5 V	85.5 H
10.7 V	1	0.99	0.47	0.74	−0.45				
10.7 H		1	0.43	0.72	−0.47				
19.3 V			1	0.86	0.81		0.67		
19.3 H				1					
21.3 V				Fig. 7	1	0.86	0.88	0.70	0.74
37 V	Fig. 7	Fig. 7	Fig. 7	Fig. 7		1	0.94	0.88	0.89
37 H	Fig. 7	Fig. 7	Fig. 7	Fig. 7			1	0.75	0.80
85.5 V	Fig. 7	Fig. 7		Fig. 7				1	0.99
85.5 H	Fig. 7	Fig. 7	Fig. 7	Fig. 7					1

Figure 10 shows the optimal combination T'_{opt} plotted against the "mean" $R'_1 \cong \sqrt{5}\ \log(R_{\text{average}})$,

$$T'_{\text{opt}} = 0.42T_{10.7H} + 0.89T_{19.3H} + 0.1T_{21.3V} - 0.06T_{37H} - 0.09T_{85.5H}, \quad (20)$$

along with selected suboptimal candidate T''s. The rms uncertainty corresponding to T'_{opt} is about 26.44%. As Fig. 10 shows, the best combination omitting the 10.7-GHz channels gives a flat plot with a σ of more than 50%. The result without the 19.3-GHz channels is not very good either.

Using T'_{opt}, the rain-retrieval results are rather encouraging. Figure 11 shows the T'_{opt}-retrieved R'_1 versus the original R'_1. There is manifestly little scatter around the diagonal. Indeed, the rms uncertainty in the R'_1 estimates is about 9%. Finally, Fig. 12 shows the T'_{opt}-reconstructed near-surface rain rate R_1 plotted against the original R_1, and Fig. 13 shows the results of the reconstruction for each of the remaining four layers R_2, . . . , R_5. Table 3 gives the precisions of the retrieved R_i in each layer. While the figures suggest that the estimates of the rain in each layer are reasonably close to their actual values, the table confirms that the relative error in the retrieval remains below 55%. These results are quite encouraging.

5. Conclusions

Our study of the joint behavior of the rain in a horizontally stratified atmosphere and the associated microwave radiances shows that the single, most crucial variable characterizing the rain profile is the vertically averaged rain rate, followed by the difference between the high-altitude subfreezing-level rain and the precipitation closer to the surface, the remaining rain eigenvariables having negligibly small variances, implying

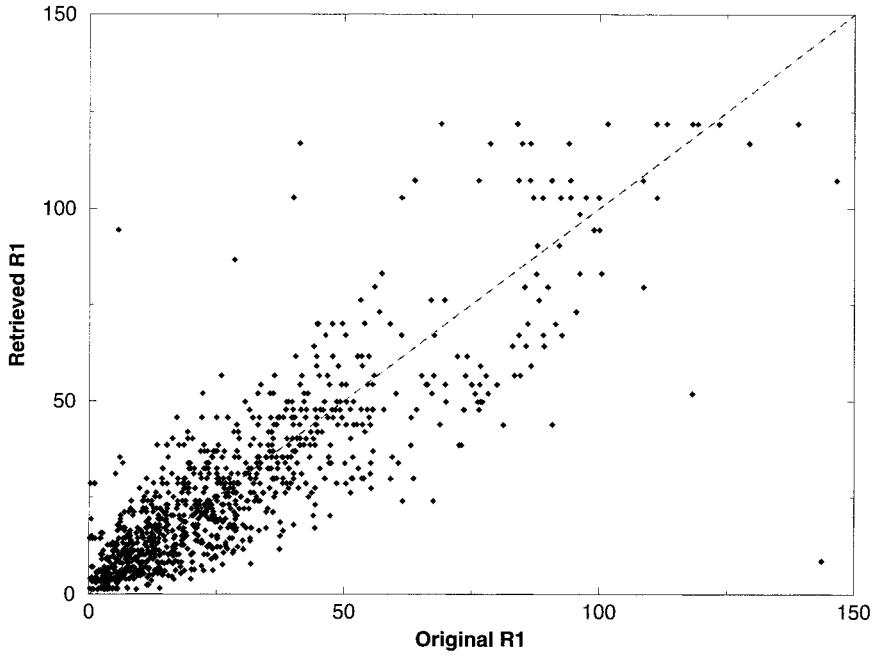

FIG. 12. The quantity R_1, retrieved from T'_{opt} and $E\{R'_2\}$, . . . , $E\{R'_5\}$, vs the actual R_1.

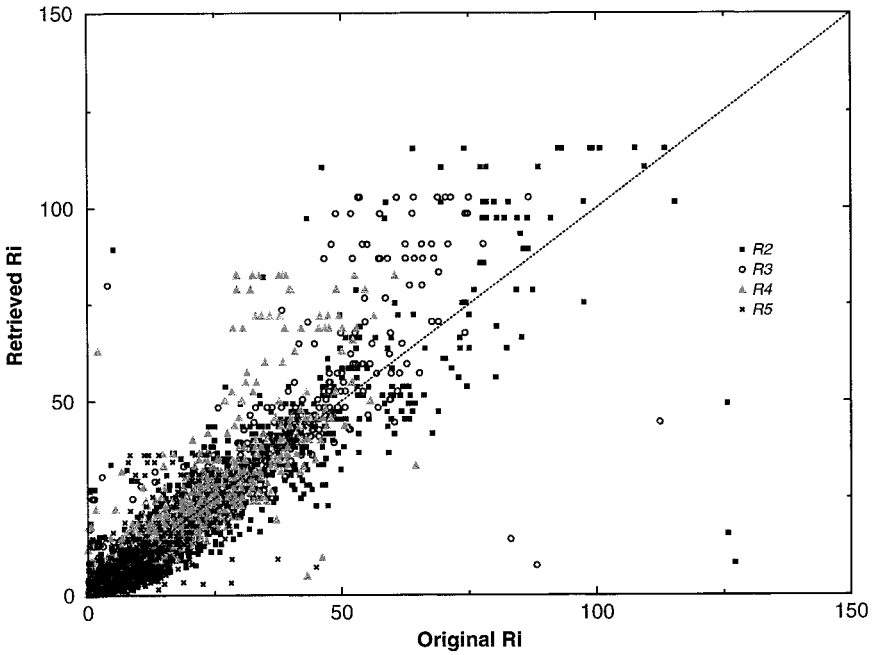

FIG. 13. The quantity R_i, retrieved from T'_{opt} and $E\{R'_2\}, \ldots, E\{R'_5\}$, vs the actual R_i's.

that they can safely be considered constant (equal to their respective means). The measurements of the passive microwave channels can similarly be described using two linear combinations of the brightness temperatures. The conditional standard deviation of the rain rates given these eigenradiances is a nearly linear function of the conditional mean rain rate when the latter is high, equal to about 55% of the rain rate, but the proportion rises to 65% when the rain is around 30 mm h^{-1} and exceeds 100% when the rain drops below 20 mm h^{-1}. The study also shows that for a higher-resolution situation, such as the case of an airborne sensor, the vertical rain rates can be adequately estimated using five of the TRMM passive-microwave channels and an associated database similar to that used for TRMM, with an rms uncertainty (due to the variations accounted for in the model database) below 55%.

Acknowledgments. Svetla Veleva is gratefully acknowledged for several helpful discussions. This work was performed at the Jet Propulsion Laboratory, California Institute of Technology, Pasedena, California, under contract with the National Aeronautics and Space Administration.

TABLE 3. Error in the rain rate calculated for each layer using the mean rain rate R'_1 estimated from T'_{opt} and using $E\{R'_2\}, \ldots, E\{R'_5\}$.

	rms deviation (in mm hr^{-1})	Mean relative error (in %)
R_1	±4.35	41.1
R_2	±3.25	29.8
R_3	±2.12	22.7
R_4	±2.27	36.3
R_5	±1.48	54.4

REFERENCES

Haddad, Z. S., E. A. Smith, C. D. Kummerow, T. Iguchi, M. R. Farrar, S. L. Durden, M. Alves, and W. S. Olson, 1997: The TRMM 'Day-1' radar-radiometer combined rain-profiling algorithm. *J. Meteor. Soc. Japan,* **75,** 799–809.

Kummerow, C. D., and L. Giglio, 1994a: A passive microwave technique for estimating rainfall and vertical structure information from space. Part I: Algorithm description. *J. Appl. Meteor.,* **33,** 3–18.

——, and ——, 1994b: A passive microwave technique for estimating rainfall and vertical structure information from space. Part II: Applications to SSM/I data. *J. Appl. Meteor.,* **33,** 19–34.

——, W. S. Olson, and L. Giglio, 1996: A simplified scheme for obtaining precipitation and vertical hydrometeor profiles from passive microwave sensors. *IEEE Trans. Geosci. Remote Sens.,* **34,** 1213–1232.

Mugnai, A., E. A. Smith, and G. J. Tripoli, 1993: Foundations for statistical-physical precipitation retrieval from passive microwave frequencies. Part II: Emission-source and generalized weighting-function properties of a time-dependent cloud-radiation model. *J. Appl. Meteor.,* **32,** 17–39.

Panegrossi, G., and Coauthors, 1998: Use of cloud microphysics for passive microwave based precipitation retrieval: Significance of consistency between model and measurement manifolds. *J. Atmos. Sci.,* **55,** 1644–1673.

Smith, E. A., A. Mugnai, H. J. Cooper, G. J. Tripoli, and X. Xiang, 1992: Foundations for statistical-physical precipitation retrieval from passive microwave frequencies. Part I: Brightness-temperature properties of a time-dependent cloud-radiation model. *J. Appl. Meteor.,* **31,** 506–531.

———, C. Kummerow, and A. Mugnai, 1994: The emergence of inversion-type profile algorithms for estimation of precipitation from satellite passive microwave measurements. *Remote Sens. Environ.,* **11,** 211–242.

Soong, S.-T., and W.-K. Tao, 1984: A numerical study of the vertical transport of momentum in a tropical rainband. *J. Atmos. Sci.*, **41,** 1049–1061.

Tesmer, J., and T. T. Wilheit, 1998: An improved microwave radiative transfer model for tropical oceanic precipitation. *J. Atmos. Sci.*, **55,** 1674–1688.

Tripoli, G. J., 1992: A nonhydrostatic model designed to simulate scale interaction. *Mon. Wea. Rev.*, **120,** 1342–1359.